



ELSEVIER

Contents lists available at ScienceDirect

Optics Communications

journal homepage: www.elsevier.com/locate/optcom

Broadband plasmon-enhanced polymer solar cells with power conversion efficiency of 9.26% using mixed Au nanoparticles

Jingyu Hao^{a,1}, Ying Xu^{a,1}, Shufen Chen^{a,*}, Yupei Zhang^a, Jiangquan Mai^b, Tsz-Ki Lau^b, Ran Zhang^b, Yang Mei^b, Lianhui Wang^b, Xinhui Lu^b, Wei Huang^{a,c}

^a Key Laboratory for Organic Electronics and Information Displays and Institute of Advanced Materials (IAM), National Synergistic Innovation Center for Advanced Materials (SICAM), Nanjing University of Posts and Telecommunications (NUPT), Nanjing 210023, PR China

^b Department of Physics, Chinese University of Hong Kong, New Territories, Hong Kong, PR China

^c Key Laboratory of Flexible Electronics (KLOFE) and Institute of Advanced Materials (IAM), National Synergistic Innovation Center for Advanced Materials (SICAM), Nanjing Tech University, 30 South Puzhu Road, Nanjing 211816, PR China

ARTICLE INFO

Article history:

Received 22 April 2015

Received in revised form

8 July 2015

Accepted 15 July 2015

Available online 30 July 2015

Keywords:

Au nanoparticle

Polymer solar cells

Localized surface plasmon resonance

Scattering

ABSTRACT

As-synthesized Au nanoparticles (NPs) composed of bone-like and rod shapes and a minority of cube and irregular spheres, generating three localized surface plasmon resonance (LSPR) peaks of 525, 575, and 775 nm, were doped into poly(3, 4-ethylenedioxythiophene):poly(4-styrenesulfonate) (PEDOT:PSS) layer and realized a power conversion efficiency of as high as 9.26% in our polymer solar cells. Optical, electrical, and morphology changes induced by Au NPs were analyzed and results demonstrate that the outstanding device performance is mainly attributed to the LSPR- and scattering-induced absorption enhancement in the active layer. Besides, mixed Au NPs also decreased the bulk resistance of PEDOT:PSS, which is found to facilitate hole transport and collection.

© 2015 Elsevier B.V. All rights reserved.

1. Introduction

Organic photovoltaic (OPV) cells are attracting a lot of attention due to their potential for high-throughput processing and low-cost. Despite the promising potential, the power conversion efficiency (PCE) of OPV is limited by the insufficient light absorption of thin active layer (~100 nm) because of the short exciton diffusion length (~10 nm) within organic materials [1]. Effective methods overcoming the exciton diffusion bottleneck include employing bulk [2,3] and mixed [4] heterojunctions and phosphorescent materials [5,6] through increasing contact interface between donors and acceptors and extending exciton's lifetime, respectively. Another feasible approach is to utilize a significantly enhanced localized field induced by surface plasmons to improve absorption of the active layer. Surface plasmons are electromagnetic surface waves confined to a metal–dielectric interface, which are either localized by metal nanoparticles (so-called localized surface plasmons) or propagated along with planar metal surfaces (so-called surface plasmon polaritons). Ag and Au are the two most frequently used materials in this area. The influences of

Ag or Au nanoparticles (NPs) or array nanostructures within carrier extraction layer or active layer on the solar cell's performances have been extensively explored by many groups [7–24]. These NPs or arrays are usually obtained by the methods of laser ablation [25,26], electron beam lithography [27], focused ion beam milling [16], scanning tunneling microscopy assisted nanostructure formation [28], wet chemical synthesis [29–31], etc. Among these approaches, wet chemical synthesis [29–31] is outstanding for the advantages of producing well-dispersed NPs in a variety of aqueous/organic solutions and the easy control over nanoparticles' shape, size, and density [32–34].

The initial explorations were mainly focused on doping a single type of Au or Ag NPs into OPV's carrier extraction layer or active layer [12–14,17,21]. In recent works, people have tried to utilize two types of NPs or a combination of metal NPs with nanostructures to enhance the device performance. For instance, Li et al. [22] used dual plasmonic nanostructures of 750 nm Ag gratings and 50 nm Au NPs to broaden active layer's absorption region and obtained a PCE of $8.79 \pm 0.15\%$ with a ~16% enhancement from $7.59 \pm 0.08\%$. In another work, Hsiao et al. [35] combined Au nanospheres (NSs) with nanorods (NRs) which resulted in two resonant peaks with the absorption ranging from visible to near infrared (NIR) region. Through systematic analysis on film's extinction and photoluminescence (PL) spectra, they concluded that the integration of two types of Au NPs with the absorption

* Corresponding author.

E-mail addresses: iamsfchen@njupt.edu.cn (S. Chen), xhlu@phy.cuhk.edu.hk (T.-K. Lau), iamdirector@fudan.edu.cn (W. Huang).

¹ These authors contributed equally to this paper.

edges covering the whole absorption spectrum is exceptionally beneficial to the performance improvements of OPVs. This idea was further extended by Lu et al. using a mixed doping of Ag and Au NPs with complementary absorption spectra [18]. A $\sim 19.6\%$ enhancement factor in PCE is realized in their polymer solar cells, much better than the results achieved by respective pure doping of Ag or Au NPs. As the best results in plasmonic OPVs [18,22], the PCEs reach 8.67% and $8.79 \pm 0.15\%$ with thieno[3,4-b]thiophene/benzodithiophene (PTB7) and poly[[4,8-bis-(2-ethyl-hexyl-thiophene-5-yl)-benzo[1,2-b:4,5-b']dithiophene-2,6-diyl]-alt-[2-(2'-ethyl-hexanoyl)-thieno[3,4-b]thiophen-4,6-diyl]] (PBDTTT-C-T) as the absorbers, respectively.

In this paper, we synthesized Au NPs with a broad absorption range of 350–1000 nm with three obvious absorption peaks of 525, 575, and 775 nm [36] covering not only the main absorption region but also the cut-off zone of the PTB7: [6,6]-phenyl-C71-butyric acid methyl ester (PC₇₁BM) active layer. We demonstrated that the mixed Au NPs with an optimal doping concentration of 4.5 vol% in the poly(3,4-ethylenedioxythiophene):poly(4-styrenesulfonate) (PEDOT:PSS) hole extraction layer (HEL) bring the PTB7:PC₇₁BM based cell significant performance enhancement factors of 17.3% and 19.8% for short-circuit current density (J_{sc}) and PCE, reaching 18.3 mA cm^{-2} and 9.26%, respectively. Our enhancement factors and PCE are among the highest reported results so far for plasmon enhanced OPV devices [13,14,21,22], especially for those using small bandgap polymer donors, e.g., PBDTTT-C-T [22] or PTB7 [18].

2. Experimental details

2.1. Synthesis of Au NPs

The Au NPs were synthesised by a seed mediated method [36].

Preparation of seed solution: 0.25 mL of a 0.01 M aqueous solution of $\text{HAuCl}_4 \cdot 3\text{H}_2\text{O}$ was added to 7.5 mL of a 0.10 M hexadecyltrimethylammonium bromide (CTAB) solution in a conical flask with a continuous stirring for 5 min. Next, 0.60 mL of an aqueous 0.01 M ice-cold NaBH_4 solution was added into the above mixed solution, following with a vigorous mixing for 2 min. The solution developed a pale brown-yellow color and was maintained in a water bath at 25 °C. This seed solution was used 2 h after its preparation.

Preparation of growth solution: 0.6 mL of a 0.01 M aqueous solution of $\text{HAuCl}_4 \cdot 3\text{H}_2\text{O}$ was added to 14.25 mL of a 0.10 M CTAB solution in a conical flask. Then 210 μl 0.01 M AgNO_3 solution was added into the above mixed solution. The resulting solution was gently mixed and stirred for 1 min. Then, 90 μl of 0.10 M ascorbic acid (AA) was added and the mixture was homogenized by stirring gently for 10 s. The solution became colorless upon addition and mixing of AA. Finally, 30 μl of seeded solution was added into the growth solution, and the final solution was left undisturbed overnight.

Au NPs were centrifugated for about three times to remove reactants and stabilizing agents and then dissolved into aqueous solution with a concentration of $\sim 10^{17}$ particles per ml before use. The aqueous solution was removed when doping these Au NPs into the PEDOT:PSS. The ultraviolet–visible (UV) spectra and the morphology for the Au NPs were measured with an ultraviolet–visible spectrophotometer (Shimadzu, UV-3600) and a transmission electron microscope (TEM) (Hitachi, HT7700). The photoluminescence (PL) spectra for the multilayer films were measured with a spectrofluorophotometer (Shimadzu, RF-5301PC).

2.2. OPVs fabrication and characteristics

Solar cells were fabricated on a 180 nm-thick indium tin oxide (ITO)-coated glass substrate. Pre-patterned ITO coated glass substrates ($7 \Omega/\text{square}$) were cleaned with acetone, ethanol, and deionized water for 10 min in sequence and then blown with a N_2 gas flow. Before spin-coating Au NPs-doped PEDOT:PSS (Baytron PVP Al 4083) layer or a control pure PEDOT:PSS layer, the substrates were treated with O_3 for 3 min. The PEDOT:PSS or PEDOT:PSS: Au NPs film was then dried at 100 °C for 20 min in a glove box with a thickness of ~ 40 nm. Different Au NPs solutions were mixed with the PEDOT:PSS aqueous solution to generate different volume ratios of Au NPs to the PEDOT:PSS solution. The co-doping solutions have been continuously stirred for several hours before spin-coating the NPs-doped PEDOT:PSS film. Electron donor material PTB7 and electron acceptor PC₇₁BM were purchased from 1-material Chemscitech and Nano C, respectively, and used as received. The PTB7 and PC₇₁BM were mixed with a weight ratio of 10–15 mg in 1 ml chlorobenzene solvent. The additive 1,8-diodoctane was then added into the PTB7:PC₇₁BM active solution with a volume ratio of 3:97. The blend layer with a stirring time of about 2 days was then spin-coated onto the PEDOT:PSS or NPs-doped PEDOT:PSS layer at a rotation rate of 1100 rpm for 60 s, forming a thin film of ~ 100 nm. The wet films were dried in covered glass petri dishes for about 0.5 h. Then the active layer-coated samples were directly transferred into the chamber without exposing air to thermally deposit a thin LiF and a thick Al cathode at 5×10^{-4} Pa, forming cells with the effective area of 0.05 cm^2 . The measurements on the current density–voltage (J – V) characteristics and the incident photon-to-electron conversion efficiency (IPCE) curves were operated using a Keithley 2400 source meter under 100 mW/cm^2 illumination (AM 1.5 G, Oriel Sol3A, 300 W) in an atmosphere environment and room temperature without further encapsulation.

2.3. Simulation work

Main contributions of different shapes and sizes Au NPs to the mixed absorption spectra in Fig. 2 have been confirmed through the calculation of the absorption cross sections (ACSSs) with a finite difference time domain (FDTD) method (FDTD software from Lumerical Solutions Inc.) [36]. Scattering cross sections (SCSSs) with and without Au NPs have also been simulated to observe the Au NPs' contribution to the light scattering in the cells. Both the ACSSs and SCSSs have been calculated with periodic boundary conditions for X and Y axes and perfectly matched layer for Z axis (assuming a distribution period of 200 nm for both X and Y axes and a non-periodic distribution for Z axis). Here, we also assumed that the longitudinal axes of the bone-like and rod shape NPs are all along with X axis or lie in the PEDOT:PSS layer. The total-field scattered-field (TFSF) light source is used to calculate ACSSs/SCSSs and both the TFSF light source and the mesh region are slightly larger than the distribution period length in X and Y directions. It is noted that the space setting for the absorption cross section is inside the TFSF light source, while that for the scattering cross section is larger than the TFSF light source. The override mesh sizes setting is 0.5, 0.5, and 0.5 nm for X, Y, and Z axes, respectively, which is small enough for getting an accurate result.

3. Results and discussion

The TEM image for these NPs is shown in Fig. 1(a). From the statistics on 400 Au NPs in the TEM image, we find that bone and rod shapes occupy a high percentage of 66%, while cube and irregular sphere shapes are 18.5% and 15.5%.

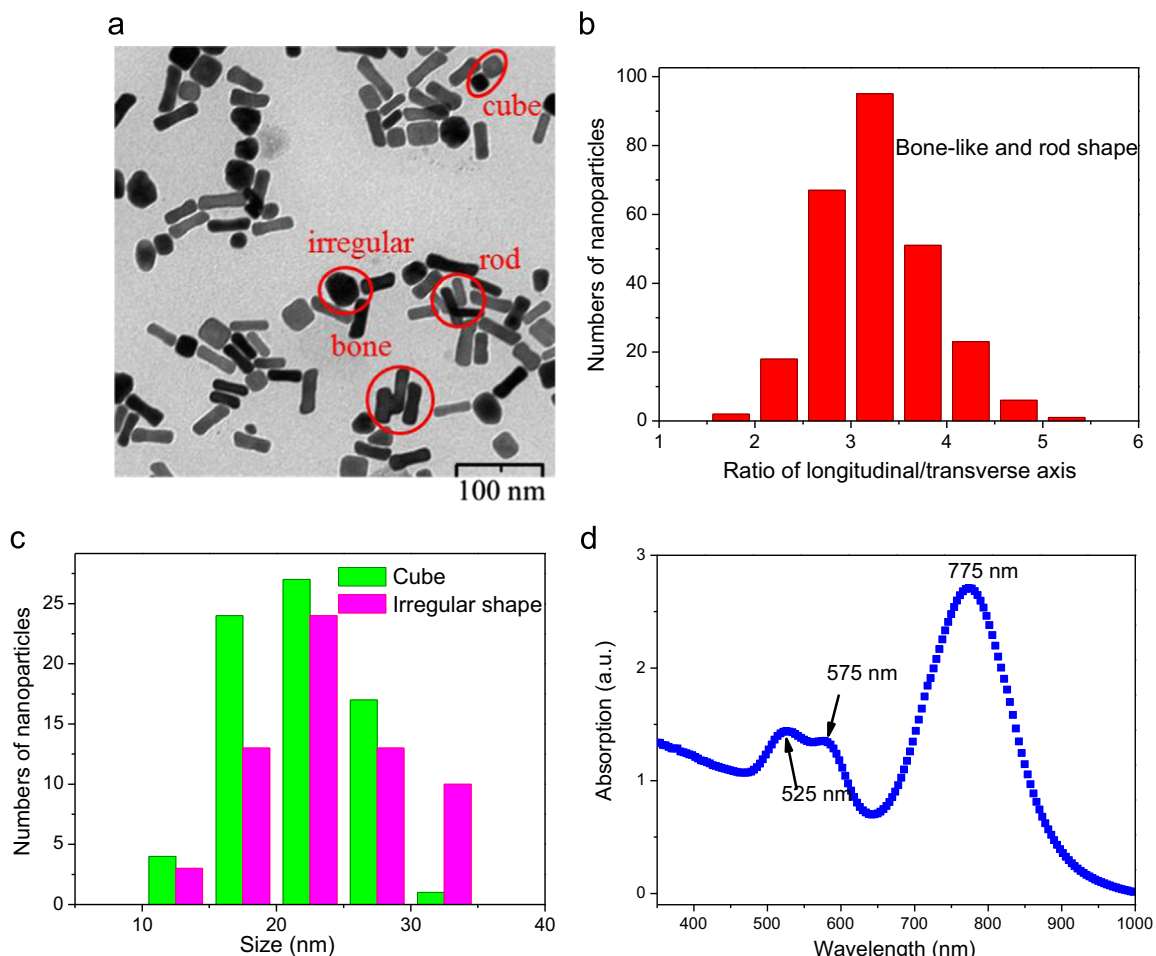


Fig. 1. The TEM image of the Au NPs (a), statistics on the numbers of bone-like and rod (b), cube and irregular shapes (c) and Au NPs from analysis on 400 particles in TEM image, and the absorption spectrum (d) for the Au NPs.

Although mixed shapes, the synthesis method still shows a good reproducibility with an only slight shift of within ± 5 nm in absorption peak if the synthesis condition is rigorous controlled. And the NPs we used here contain a majority of bone-like and rod shape with longitudinal/transverse ratios of 2.5–4.0, with detailed statistics data for different ratios being shown in the histogram of Fig. 1(b). While for cube and irregular sphere shape Au NPs, they are mainly composed of 15–30 nm side lengths/diameters, with size distributions being shown in Fig. 1(c). These mixed NPs generate wide absorption spectra covering the visible-to-NIR region with three LSPR peaks at 525, 575, and 775 nm, as Fig. 1(d) measured in aqueous solution. Simulations with a FDTD method on the ACSs of bone-like, rod and cube shape Au NPs demonstrate that the absorption around 775 and 525 nm is mainly from the longitudinal and transverse axes' resonances of both bone-like and rod shape NPs, while the 575 nm peak is mainly originated from the resonances of cube shape NPs [36]. Note that in the real devices, Au NPs were doped into the PEDOT:PSS HEL. Thus a redshift in absorption spectra should be taken into account due to a higher refractive index of PEDOT:PSS (~ 1.5) than water (~ 1.3). In order to estimate this shift, we simulated the ACSs of some representative NPs, e.g., the bone-like Au NPs with longitudinal/transverse axis of 45/13 nm and the end width of 15 nm, the rod ones with longitudinal/transverse axis of 46/12 and 40/14 nm, and the cube one with a side length of 22 nm with results shown in Fig. 2. The results indicate that the absorption spectra of bone/rods and cubes in the films show ~ 40 and ~ 55 nm redshifts compared to those in aqueous solution. That means that the

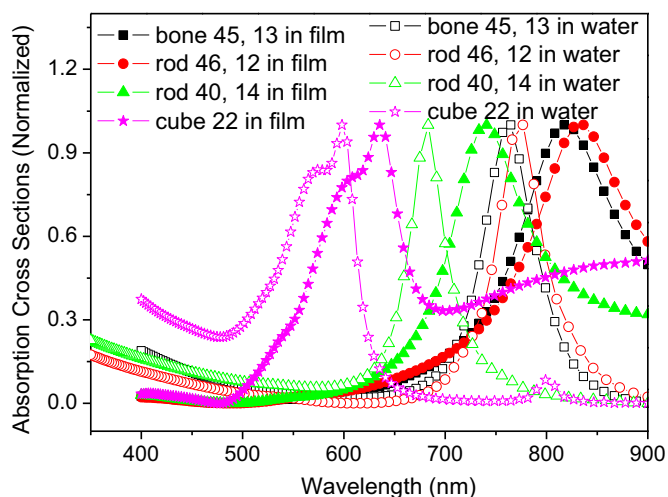


Fig. 2. Comparison the ACSs for Au NPs in the PEDOT:PSS film with those in water.

resonance peaks of ~ 575 and ~ 770 nm in aqueous solution will move to ~ 615 and ~ 825 nm in the film, respectively, covering not only the whole absorption band of PTB7: PC₇₁BM, but also its cut-off edge at ~ 800 nm. According to Hsiao's analysis [35], our mixed NPs will result in an effective absorption increase in the active layer and thereby an improvement in solar cell performance.

In order to verify our theory, a series of OPV cells were fabricated with different NP concentrations in the PEDOT:PSS HEL. The

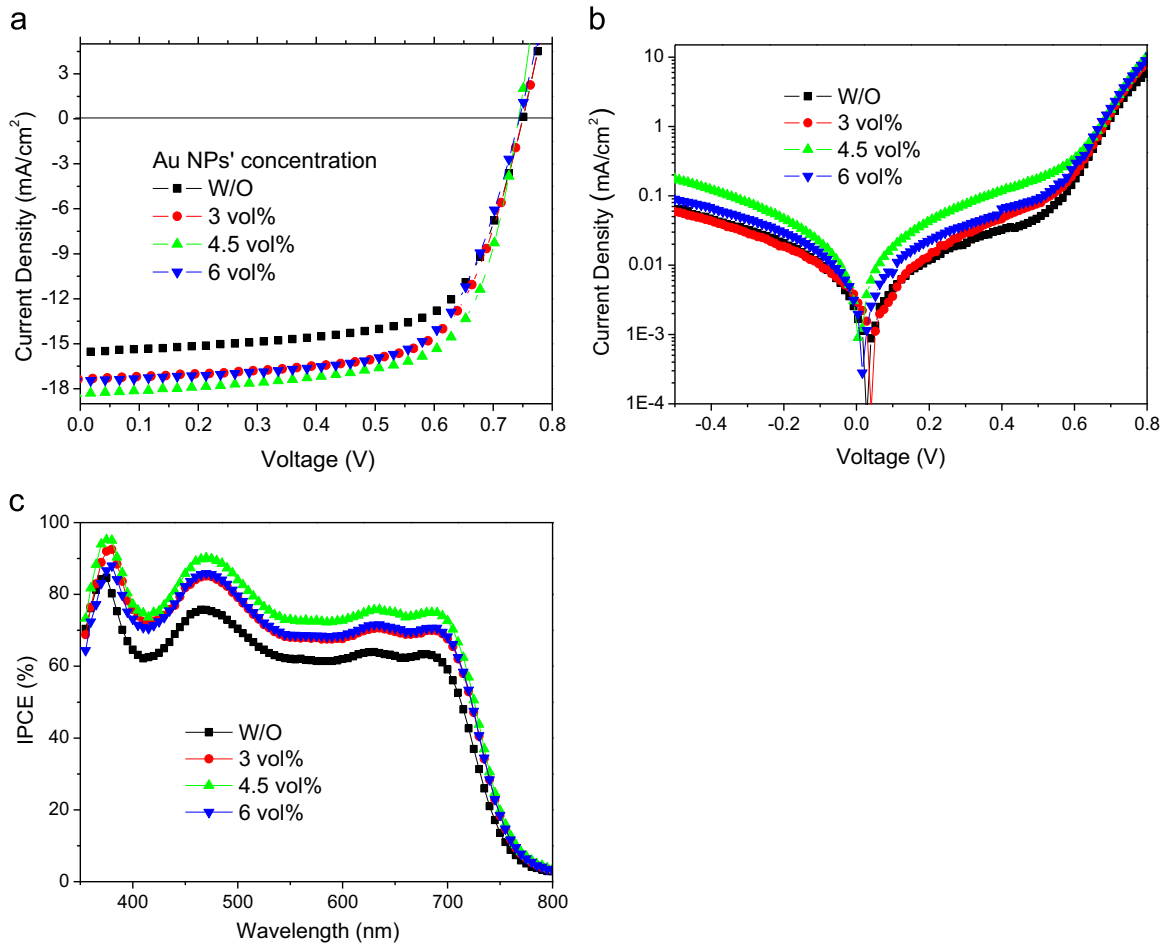


Fig. 3. J - V curves under (a) 100 mW cm^{-2} illumination and (b) dark conditions, and (c) IPCE characteristics with different Au NPs doping concentrations.

Table 1
Device photovoltaic parameters with different Au NPs doping concentrations.

| NP's concentration (vol%) | V_{oc} (V) | J_{sc} (mA/cm^2) | FF | PCE (%) | R_s (ohm cm^2) |
|---------------------------|-------------------|-------------------------------|------------------|-------------------|-----------------------------|
| W/O | 0.750 ± 0.005 | 15.6 ± 0.4 | 0.66 ± 0.01 | $7.73 \pm 0.15\%$ | 6.2 |
| 3 | 0.750 ± 0.005 | 17.3 ± 0.2 | 0.67 ± 0.01 | $8.60 \pm 0.13\%$ | 6.1 |
| 4.5 | 0.743 ± 0.005 | 18.3 ± 0.2 | 0.68 ± 0.015 | $9.17 \pm 0.09\%$ | 4.0 |
| 6 | 0.744 ± 0.005 | 17.5 ± 0.3 | 0.66 ± 0.015 | $8.73 \pm 0.15\%$ | 6.3 |

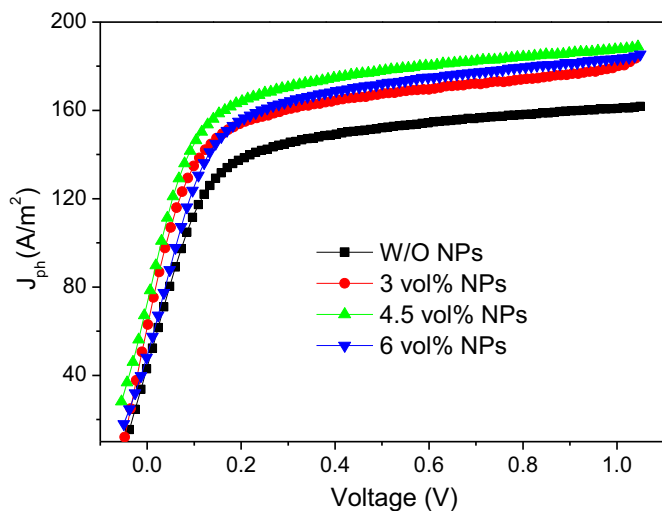


Fig. 4. Photocurrent density vs effective voltage for the OPVs with different Au NPs doping concentrations.

electrical performances for different NPs concentrations of 0, 3, 4.5, and 6 vol% under AM 1.5 illumination and dark conditions are shown in Fig. 3(a) and (b). From the J - V curves in Fig. 3(a) and the results summarized in Table 1, one finds that for the cell with an optimal doping concentration of 4.5 vol%, J_{sc} increases from 15.6 mA/cm^2 without Au NPs to 18.3 mA/cm^2 , showing a significant improvement factor of 17.3%. When deviating from the optimal doping concentration, J_{sc} begins to decrease. With a low doping concentration of below 5%, the fill factor (FF) shows a slight increase, and then gradually declines with a further increased doping ratio, with a similar trend to the previously reported results [13,37]. With the optimal NP concentration, the average PCE is $(9.17 \pm 0.09)\%$ (with a maximum of 9.26%), an improvement of $18.6 \pm 3.6\%$ from the standard device (PCE = $7.73 \pm 0.15\%$). The corresponding incident photon-to-electron conversion efficiency (IPCE) curves with different NP doping concentrations (Fig. 3(c)) exhibit an improvement in a wide wavelength ranging from 350 nm to 800 nm over that in the standard device, consistent with as-measured J - V characteristics and show a similar trend to other reports using metal NPs [12,21,38]. For comparison, we also

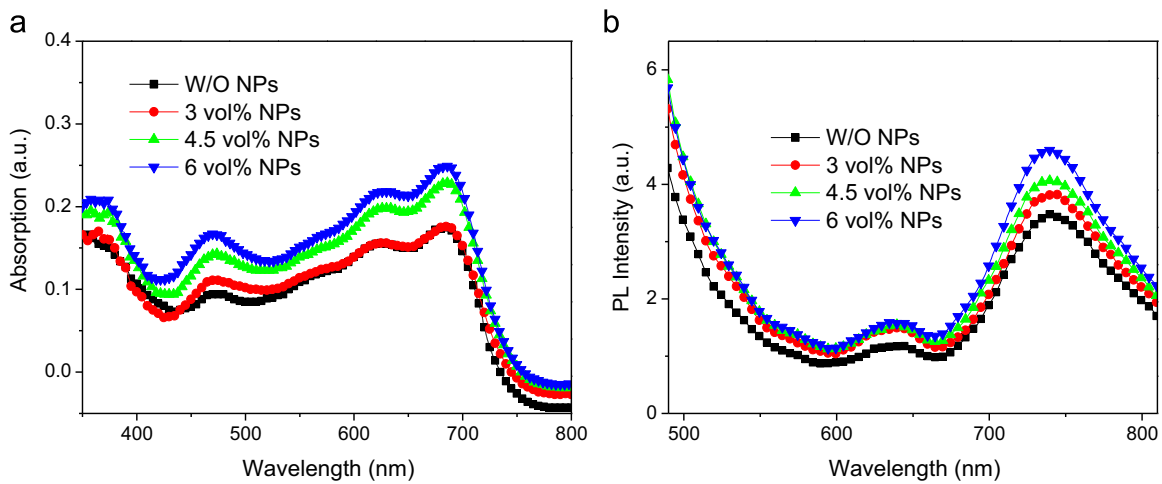


Fig. 5(a) and (b) are the measured absorption and PL spectra of the multilayer films of PEDOT:PSS: Au NPs (3, 4.5, and 6 vol%)/PTB7:PC₇₁BM and the control film of PEDOT:PSS/PTB7:PC₇₁BM.

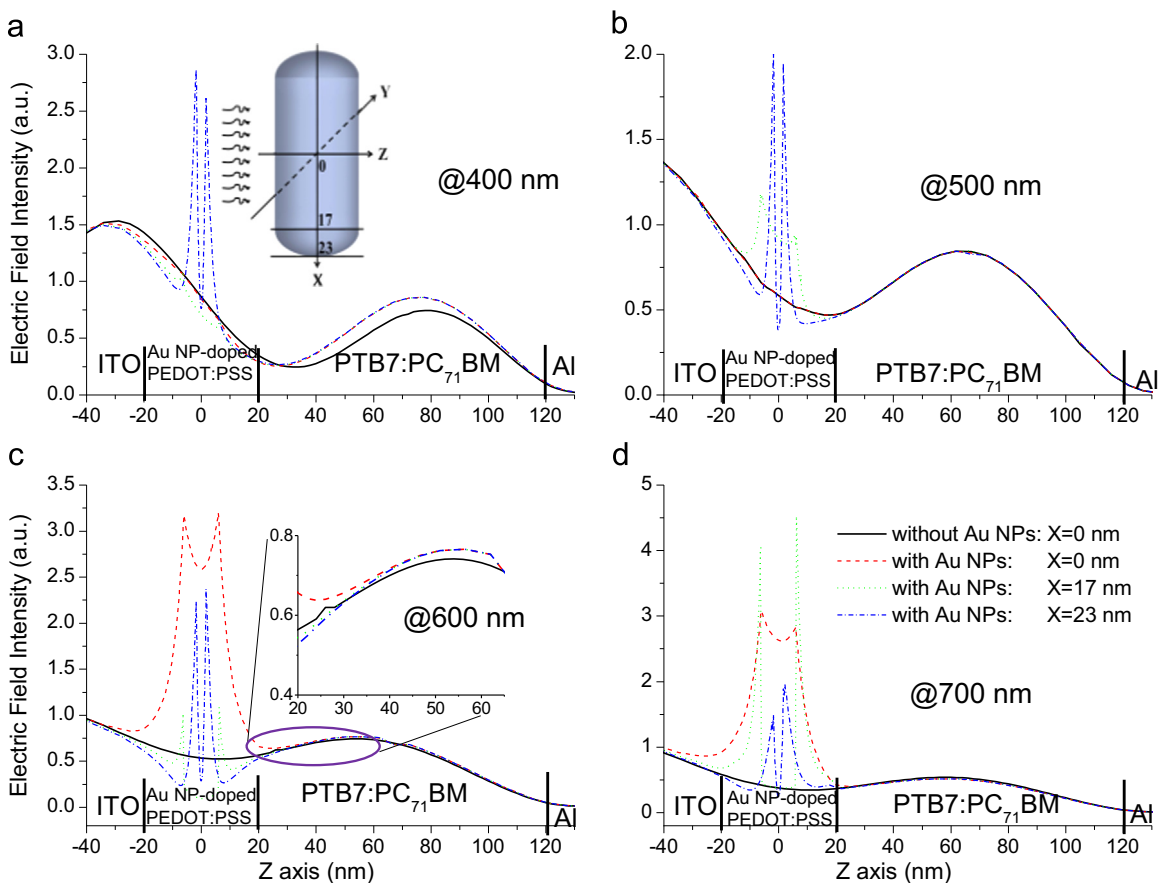


Fig. 6. Internal electric field distributions at wavelengths of (a) 400 nm, (b) 500 nm, (c) 600 nm and (d) 700 nm for devices with (dotted, dashed, dotted-dashed lines) and without Au NPs (solid lines). Inset of Fig. 6(a) is a cartoon of a Au NP in rectangular coordinate system, where Z axis is incident light propagation direction and the longitudinal axis of NPs is along X axis. Here, we calculated the field intensity distribution at X=0 (NP's center), 17 (NP's shoulder) and 23 nm (NP's end). Inset of Fig. 6(c) is the amplification in a range of 20–65 nm on Z axis.

fabricated devices with pure nanorods doped in the HEL layer. The device performances are not as good as those with mixed shape NPs, which will be published elsewhere.

Photocurrent density (J_{ph}) versus effective voltage (V_{eff}) characteristic curves were calculated to investigate photogenerated excitons (Fig. 4). Based on $J_{ph} = qG_{max}L$ (where q and L are the electronic charge and the active layer thickness), G_{max} is calculated with a 100 nm active layer thickness [39]. Assuming that all the photogenerated excitons are dissociated into free charge carriers

and collected by electrodes at a high V_{eff} region, the G_{max} values for 0, 3, 4.5, and 6 vol% NPs-doped devices are $1.01 \times 10^{28} \text{ m}^{-3}/\text{s}$, $1.13 \times 10^{28} \text{ m}^{-3}/\text{s}$, $1.18 \times 10^{28} \text{ m}^{-3}/\text{s}$, and $1.16 \times 10^{28} \text{ m}^{-3}/\text{s}$, respectively. Because the value of G_{max} is only limited by total amount of absorbed incident photons [12,40,41], the enhanced values suggest that incorporating mixed Au Doping NPs into PEDOT:PSS increases the degree of light harvesting in the active layer, which is further confirmed with a significant enhancement in the absorption spectra (Fig. 5(a)) for the multilayer films of

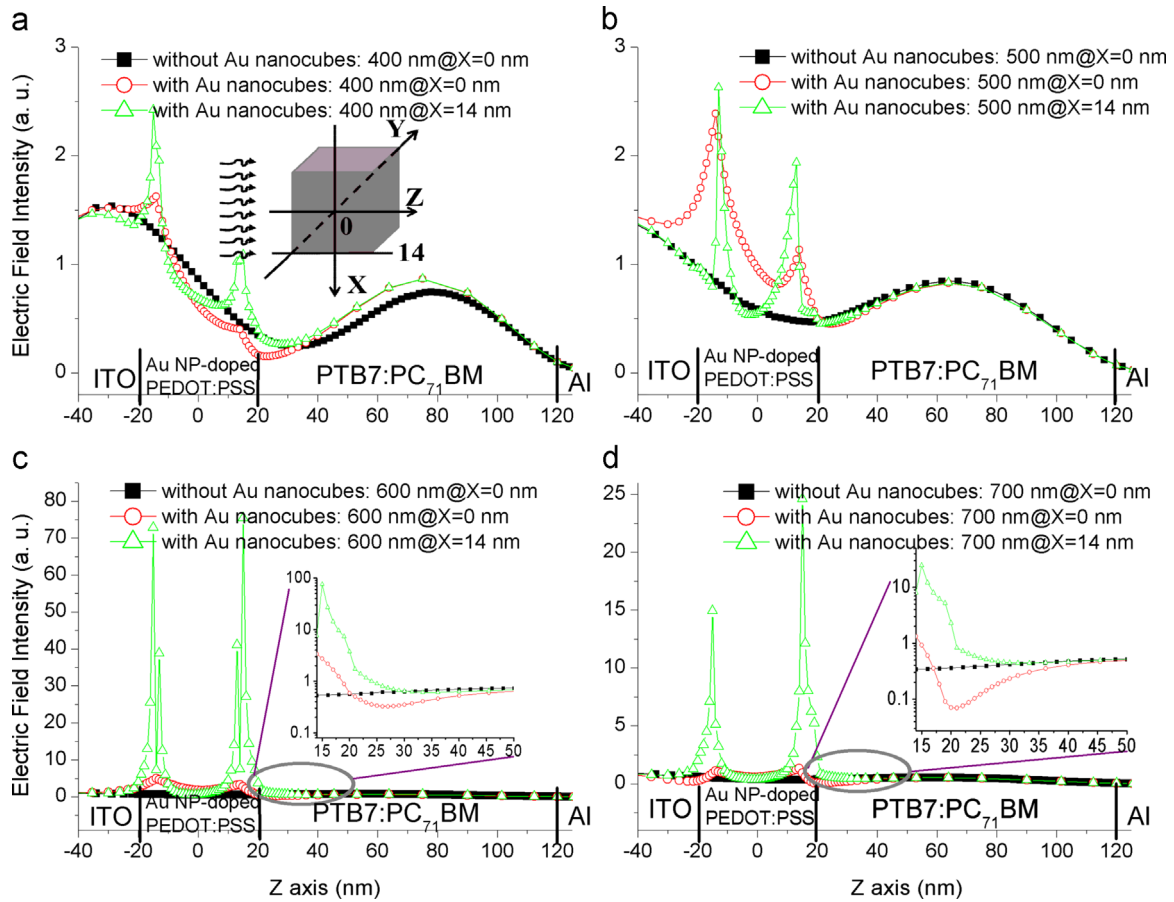


Fig. 7. Internal electric field distributions at wavelengths of (a) 400 nm, (b) 500 nm, (c) 600 nm and (d) 700 nm for devices with and without Au nanocubes. Inset of Fig. 7 (a) is a cartoon of a Au nanocube in rectangular coordinate system, where Z axis is incident light propagation direction and X axis is along with the film. Here, we calculated the field intensity distribution at X=0 (nanocube's center) and 14 nm (NP's edge). Inset of Fig. 7(c) and (d) are amplification in a range of 15–50 nm on Z axis.

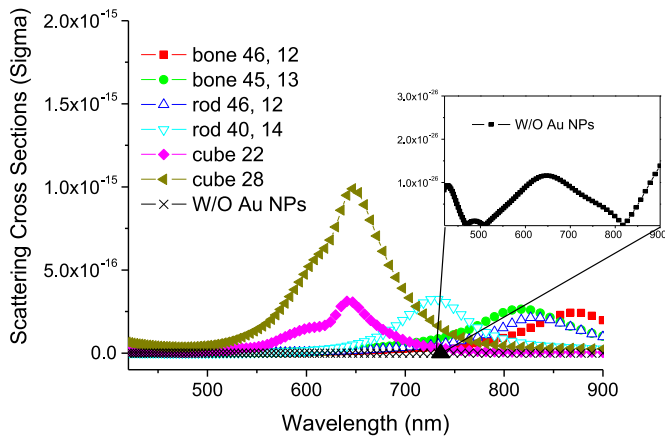


Fig. 8. Scattering cross sections for the multilayer films of glass/ITO (180 nm)/PEDOT:PSS: Au NPs (40 nm)/PTB7:PC₇₁BM (100 nm). The inset is the magnified figure for scattering cross section of the control glass/ITO/PEDOT:PSS/PTB7:PC₇₁BM multilayer.

PEDOT:PSS/NPs/PTB7:PC₇₁BM compared with the control one without NPs over a wide range of 350–800 nm. From Fig. 5(a), we also observe that the absorption magnitude continues to increase accompanied with the increase in Au NPs concentration. The measurement on the PL spectra also proves that the Au LSPR-induced absorption enhancement further brings a stronger PL intensity of the active layer, as can be seen in Fig. 5(b), indicating no direct contact between the Au NPs and the active layer.

The electromagnetic field inside the cells was calculated in

order to study the influence of Au NPs on internal light field inside devices. Due to a far larger intensity for the electric field than the magnetic field, only electric field intensity is given in Fig. 6. And since bone-like shape Au NPs show a similar local field characteristic with Au nanorods if they have the same longitudinal/transverse ratio, here only Au nanorods were simulated. Using Au NPs causes a different localized field enhancement around NPs at the wavelengths of 400, 500, 600, 700 nm and at different positions on X axis. Here, a Au nanorod with longitudinal and transverse axes of 46 and 12 nm is used for simulation, where 0, 17, and 23 nm that correspond to nanorod's center, shoulder and end. Inset of Fig. 6(a) is a cartoon of a Au NP in rectangular coordinate system, where Z axis is along the incident light propagation direction and perpendicular to the film. Here, considering of most nanorods lie in the film (deduced from SEM image), the longitudinal axis of Au nanorod is perpendicular to Z axis. From Fig. 6 (a), Au NP induces an increase in internal field almost in the whole PTB7:PC₇₁BM active layer at 400 nm with a factor of 16.6% by integrating the electric field in the active layer (from 20–120 nm on X axis). In contrast, the electric field in the active layer shows a negligible change at other wavelengths, e.g., 500–700 nm. Besides, one finds that the electric fields at 600 and 700 nm not only show significant enhancements around the NPs but also extend into the active layer. For instance, at the center of Au NPs (X=0), the electric field doping with Au NPs keeps a higher intensity from –20 to 65 nm than that without NPs due to LSPR directly from NPs (Inset of Fig. 6(c)). In the case of 700 nm, at both X=0 and 17 nm it occurs the phenomenon of the enhanced field in the PTB7:PC₇₁BM layer although the field decreases rapidly. Similar

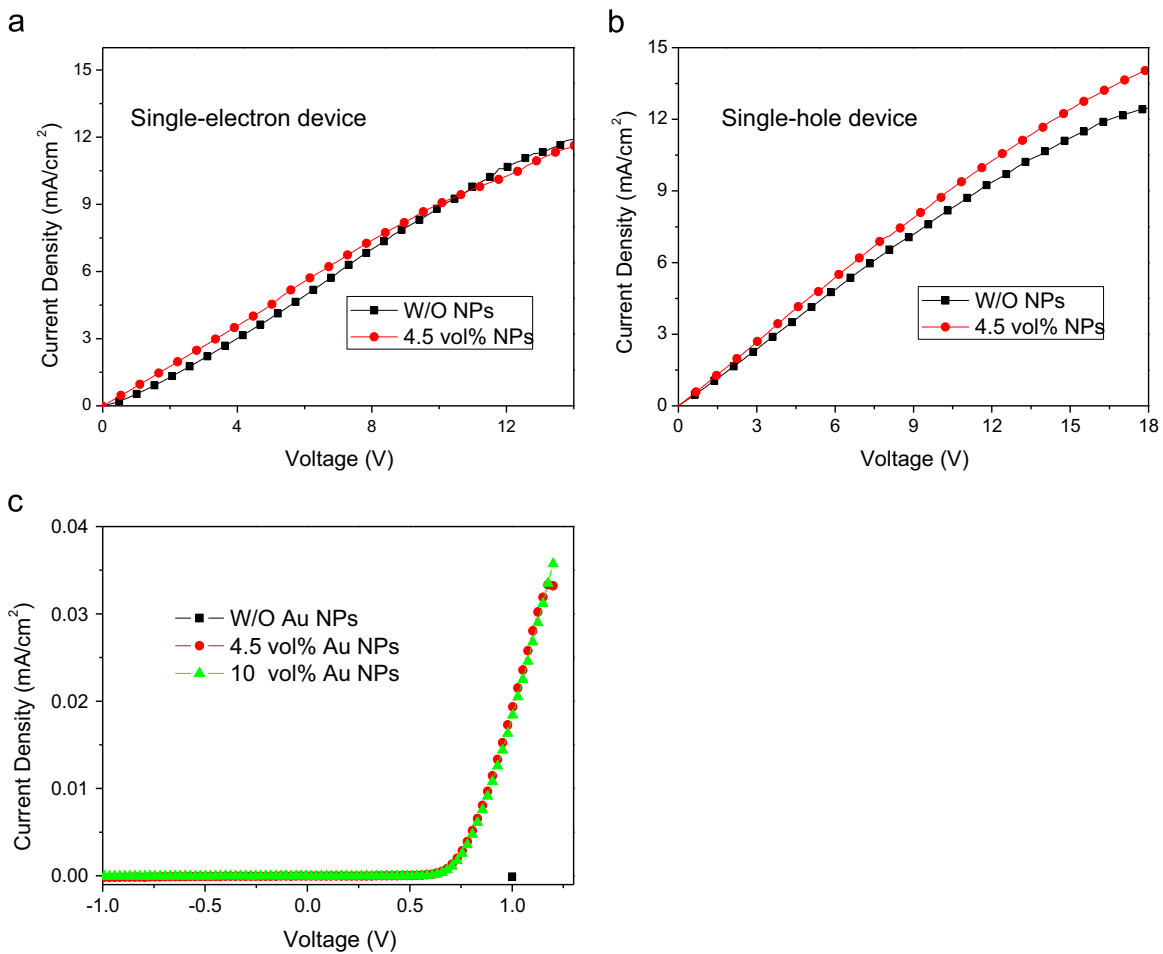


Fig. 9. The J - V characteristics for (a) single-electron and (b) single-hole devices. (c) Current injection density vs voltage for the OPVs with Au NPs directly spincast onto the ITO anode.

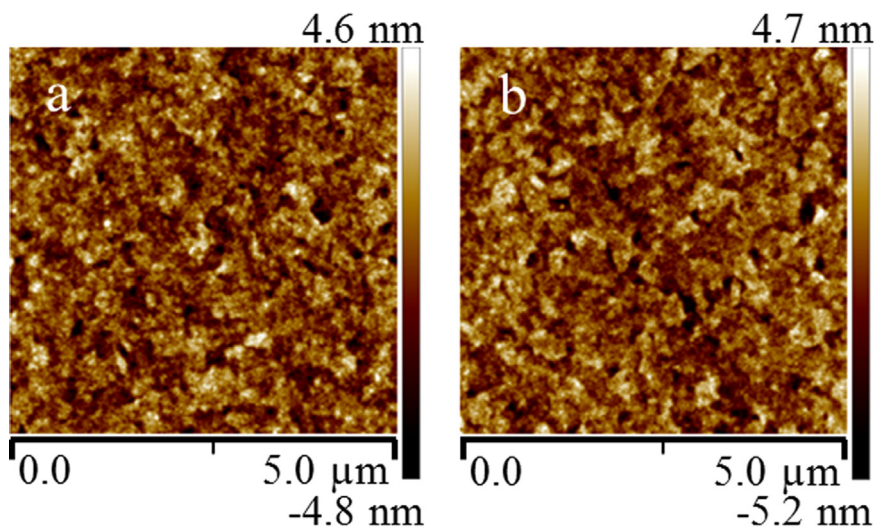


Fig. 10. The surface AFM images for (a) the pure PEDOT:PSS film ($R_a=1.05$) and (b) 4.5 vol% Au NPs-doped PEDOT:PSS film ($R_a=1.11$).

enhancements in electric field around Au nanocube are also observed not only at 400 nm in the whole active layer but also at 600 and 700 nm in the active layer near Au nanocube, as shown in Fig. 7. Note that the electric field enhancement induced by Au nanocube is much more significant than that by Au nanorod. Analysis on the results indicates that the increase in the internal light field is very beneficial to the improvement of the active

layer's absorption, thus resulting in the J_{sc} and PCE increase.

Beside Au NPs-induced absorption and light field change in the active layer, it should be noted that light scattering from these Au NPs also gives rise to a longer light path and thereby a further improved light absorption in OPV cells. To study scattering influence from these Au NPs, we simulated the scattering cross sections of primary Au NPs with the FDTD software. The detailed parameter

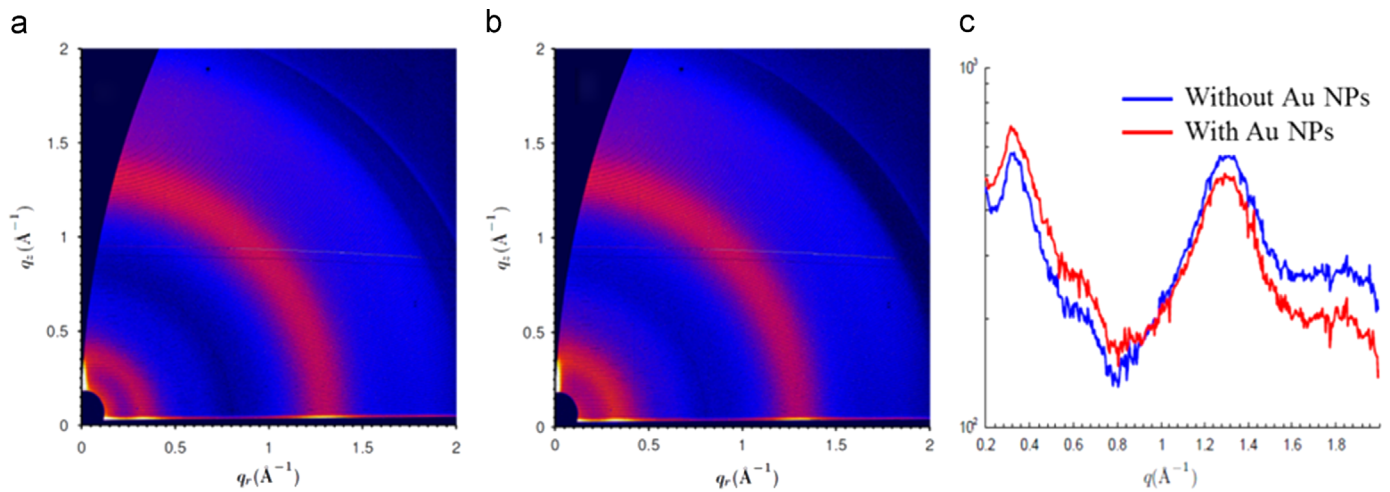


Fig. 11. The GIWAXS patterns of PTB7:PC₇₁BM thin films on the PEDOT:PSS layer (a) with 4.5 vol% and (b) without Au NPs. (c) The corresponding intensity integrals vs q along horizontal axis.

settings are described in experimental details. Compared to the control cell without Au NPs, scatterings from Au NPs with bone-like, rod, and cube shapes give significant enhancement factors of 10^{10} – 10^{11} (Fig. 8), indicating a substantial contribution from NP light scattering.

Other possible factors, e.g., changes in the hole extraction and transport ability and morphology induced by Au NPs, may also influence the device performance. In order to investigate the Au NPs influence on the hole extraction and transport ability of the PEDOT:PSS film, single-hole and single-electron devices with the structures of ITO/PEDOT:PSS (~ 40 nm, with 4.5 vol% or without Au NPs)/Al and ITO/LiF (1 nm)/PEDOT:PSS (~ 40 nm, with 4.5 vol% or without Au NPs)/LiF/Al were fabricated.

The J - V curves shown in Fig. 9(a) and (b) indicate that the incorporation of Au NPs does not obviously affect the electron injection/transport ability of the PEDOT:PSS film, however, their occurrence improves the hole current in the hole-dominated device. It may be attributed to a slightly higher work function of Au (5.4 eV) than the highest occupied molecular orbital (~ 5.2 eV) of PEDOT:PSS, providing a better hole injection at the ITO/PEDOT:PSS interface [42,43]. However, this explanation is excluded by the unchanged injected current for devices with Au NPs spin-cast directly onto ITO (Fig. 9(c)). Thus Au-induced shallow impurity energy levels [42,43] in the PEDOT:PSS film play an important role in increasing hole transport and decreasing the bulk resistance of PEDOT:PSS (from 1250 to 1150 Ω cm²) and this point is also supported with the dark J - V curves in Fig. 3(b), in which the Au NPs-doped cells show higher current densities than the standard one.

As shown in Fig. 10, the morphology changes of the PEDOT:PSS layer with 4.5 vol% and without Au NPs were measured by applying atomic force microscopy (AFM) on the surface of the PEDOT:PSS and PEDOT:PSS:Au NPs films. With the utilization of the Au NPs, we observe a slight change of the surface morphology for the NPs-doped PEDOT:PSS film, with an increase in surface roughness (R_a) from 1.05 nm to 1.11 nm. This slightly increased anode surface roughness does not significantly increase the interface area of the anode/active layer and not reduce the hole travelling routes towards the anode, thus no obvious J_{sc} increase induced by the film's surface roughness. Grazing incidence wide-angle X-ray scattering measurements were also carried out at Beamline 23 A at the National Synchrotron Radiation Research Center, Hsinchu with a 10 keV beam in order to investigate the effect of Au NPs doping on the molecular packing within the active layer [44]. Scattering patterns for the active layer on PEDOT:PSS films with and without Au NPs (Fig. 11) exhibit similar features with PTB7 (100) lamellar

ring located at $q \approx 0.32$ \AA^{-1} and PC₇₁BM amorphous ring at $q \approx 1.32$ \AA^{-1} . There are no obvious changes in scattering ring intensity, position and width, which suggest that no significant molecular packing change is induced by Au NP doping.

4. Conclusion

In conclusion, the as-synthesized Au NPs generate wide absorption spectra of 350–1000 nm due to mixed bone-like, rod, and cube shapes. We doped these NPs into the PEDOT:PSS HEL to improve photovoltaic performance in PTB7:PC₇₁BM based solar cell. With the optimal doping concentration of 4.5%, the best performing cell achieves a J_{sc} of 18.3 mA cm⁻² and a PCE of 9.26%, 17.3% and 19.8% enhancement compared to the standard sample without Au NPs doping, the highest reported so far for plasmonic polymer solar cells to our knowledge. Detailed optical, electrical, and morphological characterizations indicated that the cell performance improvement is mainly due to the LSPR- and scattering-induced absorption enhancement of the active layer. Au doping-induced bulk resistance decrease of poly(3,4-ethylenedioxythiophene):poly(4-styrenesulfonate) is found to facilitate exciton dissociation, hole transport and collection. This study suggests an efficient route to further push the PCE of high-efficiency solar cells made of low bandgap co-polymer with mixed shape Au NPs for wide-spectra plasmonic enhancement.

Acknowledgments

The authors acknowledge financial support from the Ministry of Science and Technology (973 project, Grant nos. 2015CB932202 and 2012CB933301), National Natural Science Foundation of China (Grant nos. 61274065, 51173081, 61136003 and BZ2010043), the Ministry of Education of China (No. IRT1148), the Key Project of Chinese Ministry of Education (Grant nos. 104246, and 707032), the National Natural Science Foundation of Jiangsu Province (Grant no. BM2012010), the Priority Academic Program Development of Jiangsu Higher Education Institutions (Grant no. YX03001), the National Synergistic Innovation Center for Advanced Materials and the Synergetic Innovation Center for Organic Electronics and Information Displays of Jiangsu Province. J.Q.M, T.K.L and X.H.L acknowledge the financial support from CUHK Direct Grant no. 4053075 and Focused Innovation Scheme B Grant "Centre for Solar Energy Research" (Grant no. 1902034).

References

- [1] P. Peumans, A. Yakimov, S.R. Forrest, Small molecular weight organic thin-film photodetectors and solar cells, *J. Appl. Phys.* 93 (2003) 3693–3723.
- [2] J.J.M. Halls, C.A. Walsh, N.C. Greenham, E.A. Marseglia, R.H. Friend, S.C. Moratti, A.B. Holmes, Efficient photodiodes from interpenetrating polymer networks, *Nature* 376 (1995) 498–500.
- [3] P. Peumans, S. Uchida, S.R. Forrest, Efficient bulk heterojunction photovoltaic cells using small-molecular-weight organic thin films, *Nature* 425 (2003) 158–162.
- [4] J. Xue, B.P. Rand, S. Uchida, S.R. Forrest, A hybrid planar-mixed molecular heterojunction photovoltaic cell, *Adv. Mater.* 17 (2005) 66.
- [5] G. Yu, J. Gao, J.C. Hummelen, F. Wudl, A.J. Heeger, Polymer photovoltaic cells: enhanced efficiencies via a network of internal donor-acceptor heterojunctions, *Science* 270 (1995) 1789–1791.
- [6] Y. Shao, Y. Yang, Efficient organic heterojunction photovoltaic cells based on triplet materials, *Adv. Mater.* 17 (2005) 2841.
- [7] O. Stenzel, A. Stendal, K. Voigtsberger, C. von Borczyskowski, Enhancement of the photovoltaic conversion efficiency of copper phthalocyanine thin film devices by incorporation of metal clusters, *Sol. Energy Mater. Sol. Cells* 37 (1995) 337–348.
- [8] M. Westphalen, U. Kreibitz, J. Rostalski, H. Lüth, D. Meissner, Metal cluster enhanced organic solar cells, *Sol. Energy Mater. Sol. Cells* 61 (2000) 97–105.
- [9] B.P. Rand, P. Peumans, S.R. Forrest, Long-range absorption enhancement in organic tandem thin-film solar cells containing silver nanoclusters, *J. Appl. Phys.* 96 (2004) 7519–7526.
- [10] K. Tvingstedt, N.-K. Persson, O. Inganäs, A. Rahachou, Surface plasmon increase absorption in polymer photovoltaic cells, *Appl. Phys. Lett.* 91 (2007) 113514.
- [11] N.C. Lindquist, W.A. Luhman, S.-H. Oh, R.J. Holmes, Plasmonic nanocavity arrays for enhanced efficiency in organic photovoltaic cells, *Appl. Phys. Lett.* 93 (2008) 123308.
- [12] F.C. Chen, J.L. Wu, C.L. Lee, Y. Hong, C.H. Kuo, M.H. Huang, Plasmonic-enhanced polymer photovoltaic devices incorporating solution-processable metal nanoparticles, *Appl. Phys. Lett.* 95 (2009) 013305.
- [13] J.H. Lee, J.H. Park, J.S. Kim, D.Y. Lee, K. Cho, High efficiency polymer solar cells with wet deposited plasmonic gold nanodots, *Org. Electron.* 10 (2009) 416–420.
- [14] J.-L. Wu, F.-C. Chen, Y.-S. Hsiao, F.-C. Chien, P. Chen, C.-H. Kuo, M.H. Huang, C.-S. Hsu, Surface plasmonic effects of metallic nanoparticles on the performance of polymer bulk heterojunction solar cells, *ACS Nano* 5 (2011) 959–967.
- [15] A.P. Kulkarni, K.M. Noone, K. Munechika, S.R. Guyer, D.S. Ginger, Plasmon-enhanced charge carrier generation in organic photovoltaic films using silver nanoprisms, *Nano Lett.* 10 (2010) 1501–1505.
- [16] Y.C. Chang, F.Y. Chou, P.H. Yeh, H.W. Chen, S.H. Chang, Y.C. Lan, T.F. Guo, T. C. Tsai, C.T. Lee, Effects of surface plasmon resonant scattering on the power conversion efficiency of organic thin-film solar cells, *J. Vac. Sci. Technol. B* 25 (2007) 1899–1902.
- [17] D.H. Wang, D.Y. Kim, K.W. Choi, J.H. Seo, S.H. Im, J.H. Park, O.O. Park, A. J. Heeger, Enhancement of donor-acceptor polymer bulk heterojunction solar cell power conversion efficiencies by addition of Au nanoparticles, *Angew. Chem. Int. Ed.* 50 (2011) 5519–5523.
- [18] L.Y. Lu, Z.Q. Luo, T. Xu, L.P. Yu, The role of N-doped multiwall carbon nanotubes in achieving highly efficient polymer bulk heterojunction solar cells, *Nano Lett.* 13 (2013) 2365–2369.
- [19] L. Qiao, D. Wang, L. Zuo, Y. Ye, J. Qian, H. Chen, S. He, Localized surface plasmon resonance enhanced organic solar cell with gold nanospheres, *Appl. Energy* 88 (2011) 848–852.
- [20] J. Yang, J.B. You, C.C. Chen, W.C. Hsu, H.R. Tan, X.W. Zhang, Z.R. Hong, Y. Yang, Plasmonic polymer tandem solar cell, *ACS Nano* 5 (2011) 6210–6217.
- [21] D.D.S. Fung, L. Qiao, W.C.H. Choy, C. Wang, W.E.I. Sha, F. Xie, S. He, Optical and electrical properties of efficiency enhanced polymer solar cells with Au nanoparticles in a PEDOT-PSS layer, *J. Mater. Chem.* 21 (2011) 16349.
- [22] X. Li, W.C.H. Choy, L. Huo, F. Xie, W.E.I. Sha, B. Ding, X. Guo, Y. Li, J. Hou, J. You, Y. Yang, Dual plasmonic nanostructures for high performance inverted organic solar cells, *Adv. Mater.* 24 (2012) 3046–3052.
- [23] X. Li, W.C.H. Choy, H. Lu, W.E.I. Sha, A.H.P. Ho, Efficiency enhancement of organic solar cells by using shape-dependent broadband plasmonic absorption in metallic nanoparticles, *Adv. Funct. Mater.* 23 (2013) 2728–2735.
- [24] S.F. Chen, F. Cheng, Y. Mei, B. Peng, M. Kong, J.Y. Hao, R. Zhang, Q.H. Xiong, L. H. Wang, W. Huang, Plasmon-enhanced polymer photovoltaic cells based on large aspect ratio gold nanorods and the related working mechanism, *Appl. Phys. Lett.* 104 (2014) 213903.
- [25] C.D. Chen, Y.T. Yeh, C.R.C. Wang, The fabrication and photo-induced melting of networked gold nanostructures and twisted gold nanorods, *J. Phys. Chem. Solids* 62 (2001) 1587–1597.
- [26] J. Bosbach, D. Martin, F. Stietz, T. Wenzel, F. Trager, Laser-based method for fabricating monodisperse metallic nanoparticles, *Appl. Phys. Lett.* 74 (1999) 2605–2607.
- [27] N. Felidj, J. Aubard, G. Levi, J.R. Krenn, M. Salerno, G. Schider, B. Lamprecht, A. Leitner, F.R. Aussenegg, Controlling the optical response of regular arrays of gold particles for surface-enhanced Raman scattering, *Phys. Rev. B* 65 (2002) 075419.
- [28] D.M. Kolb, R. Ullmann, T. Will, Nanofabrication of small copper clusters on gold(111) electrodes by a scanning tunneling microscope, *Science* 275 (1997) 1097–1099.
- [29] N.R. Jana, L. Gearheart, C.J. Murphy, Wet chemical synthesis of silver nanorods and nanowires of controllable aspect ratio, *Chem. Commun.* 7 (2001) 617–618.
- [30] N.R. Jana, L. Gearheart, C.J. Murphy, Wet chemical synthesis of high aspect ratio cylindrical gold nanorods, *J. Phys. Chem. B* 105 (2001) 4065–4067.
- [31] C.H. Walker, J.V. St. John, P. Wisian-Neilson, Synthesis and size control of gold nanoparticles stabilized by poly(methylphenylphosphazene), *J. Am. Chem. Soc.* 123 (2001) 3846–3847.
- [32] B. Nikoobakht, M.A. El-Sayed, Surface-enhanced Raman scattering studies on aggregated gold nanorods, *J. Phys. Chem. A* 107 (2003) 3372–3378.
- [33] W.A. Murray, W.L. Barnes, Plasmonic materials, *Adv. Mater.* 19 (2007) 3771–3782.
- [34] M. Pelton, J. Aizpurua, G. Bryant, Metal-nanoparticle plasmonics, *Laser Photonics Rev.* 2 (2008) 136–159.
- [35] Y.-S. Hsiao, S. Charan, F.-Y. Wu, F.-C. Chien, C.-W. Chu, P. Chen, F.-C. Chen, Improving the light trapping efficiency of plasmonic polymer solar cells through photon management, *J. Phys. Chem. C* 116 (2012) 20731–20737.
- [36] Y.P. Zhang, J.Y. Hao, X. Li, S.F. Chen, L.H. Wang, X.A. Li, W. Huang, Plasmonic-enhanced polymer photovoltaic cells based on Au nanoparticles with wide absorption spectra of 300–1000 nm, *J. Mater. Chem. C* 2 (2014) 9303–9310.
- [37] X.Q. Chen, L.J. Zuo, W.F. Fu, Q.X. Yan, C.C. Fan, H.Z. Chen, Insight into the efficiency enhancement of polymer solar cells by incorporating gold nanoparticles, *Sol. Energy Mater. Sol. Cells* 111 (2013) 1–8.
- [38] S.-S. Kim, S.-I. Na, J. Jo, D.-Y. Kim, Y.-C. Nah, Plasmon enhanced performance of organic solar cells using electrodeposited Ag nanoparticles, *Appl. Phys. Lett.* 93 (2008) 073307.
- [39] V.D. Mihailetchi, J. Wildeman, P.W.M. Blom, Space-charge limited photocurrent, *Phys. Rev. Lett.* 94 (2005) 126602.
- [40] V.D. Mihailetchi, L.J.A. Koster, J.C. Hummelen, P.W.M. Blom, Photocurrent generation in polymer-fullerene bulk heterojunctions, *Phys. Rev. Lett.* 93 (2004) 216601–216604.
- [41] V.D. Mihailetchi, H.X. Xie, B. de Boer, L.J.A. Koster, P.W.M. Blom, Charge transport and photocurrent generation in poly(3-hexylthiophene): methanofullerene bulk-heterojunction solar cells, *Adv. Funct. Mater.* 16 (2006) 699–708.
- [42] K. Kim, D.L. Carroll, High-efficiency photovoltaic devices based on annealed poly(3-hexylthiophene) and 1-(3-methoxycarbonyl)-propyl-1-phenyl-(6,6)C-61 blends, *Appl. Phys. Lett.* 87 (2005) 203113.
- [43] C.C.D. Wang, W.C.H. Choy, C. Duan, D.D.S. Fung, W.E.I. Sha, F.-X. Xie, F. Huang, Y. Cao, Optical and electrical effects of gold nanoparticles in the active layer of polymer solar cells, *J. Mater. Chem.* 22 (2012) 1206–1211.
- [44] T. Xiao, H. Xu, G. Grancini, J. Mai, A. Petrozza, U.-S. Jeng, Y. Wang, X. Xin, Y. Lu, N. Choon, H. Xiao, B. Ong, X. Lu, N. Zhao, Molecular packing and electronic processes in amorphous-like polymer bulk heterojunction solar cells with fullerene intercalation, *Sci. Rep.* 4 (2014) 5211.